Scientific Computing manuscript No.
(will be inserted by the editor)

A stabilized separation of variables method for the modified biharmonic equation

T. Askham

Abstract The modified biharmonic equation is encountered in a variety of application areas, including streamfunction formulations of the Navier-Stokes equations. We develop a separation of variables representation for this equation in polar coordinates, for either the interior or exterior of a disk, and derive a new class of special functions which makes the approach stable. We discuss how these functions can be used in conjunction with fast algorithms to accelerate the solution of the modified biharmonic equation or the "bi-Helmholtz" equation in more complex geometries.

Keywords separation of variables · modified biharmonic equation · special functions · integral equation · fast multipole method

1 Introduction

Many fourth order elliptic partial differential equations of physical interest can be expressed in terms of the composition of two second order elliptic differential operators. We focus here on the modified biharmonic equation in two dimensions, but much of what follows can be applied to other equations, such as the bi-Helmholtz equation, and has a natural extension to the three dimensionsal setting. In a domain Ω with boundary $\partial\Omega$, the modified biharmonic equation can be written in the form

$$(\Delta^2 - \lambda^2\Delta)u = \Delta(\Delta - \lambda^2)u = 0 \text{ in } \Omega \,, \tag{1}$$

with $\lambda \in \mathbb{R}$, subject to two application-specific, boundary conditions. This equation arises naturally when solving the the Navier-Stokes equations using an implicit marching scheme [7,15,8,4,18].

The Green's function for the governing equation is [18]

$$\mathscr{G}(r) = -\frac{1}{2\pi\lambda^2}\left(\log r + K_0(\lambda r)\right) \,.$$

T. Askham's work was supported by the Office of the Assistant Secretary of Defense for Research and Engineering and AFOSR under NSSEFF Program Award FA9550-10-1-0180 and the Office of the Assistant Secretary of Defense for Research and Engineering and AFOSR under award FA95550-15-1-0385.

T. Askham
University of Washington, Lewis Hall, 4182 W Stevens Way NE, Seattle, WA 98195-3925
E-mail: askham@uw.edu

Applying Green's identities, we obtain, for u a solution of (1),

$$u(\mathbf{x}) = \int_{\partial\Omega} \partial_n \Delta_y \mathscr{G}(\mathbf{x},\mathbf{y}) u(\mathbf{y}) - \Delta_y \mathscr{G}(\mathbf{x},\mathbf{y}) \partial_n u(\mathbf{y}) + \partial_n \mathscr{G}(\mathbf{x},\mathbf{y}) \Delta_y u(\mathbf{y}) - \mathscr{G}(\mathbf{x},\mathbf{y}) \partial_n \Delta_y u(\mathbf{y}) - \lambda^2 \left(\partial_n \mathscr{G}(\mathbf{x},\mathbf{y}) u(\mathbf{y}) - \mathscr{G}(\mathbf{x},\mathbf{y}) \partial_n u(\mathbf{y})\right) dS(\mathbf{y}) \,,$$

where ∂_ν denotes differentiation in the normal direction and $\mathscr{G}(\mathbf{x},\mathbf{y}) = \mathscr{G}(|\mathbf{x}-\mathbf{y}|)$. Therefore, u is representable in terms of layer potentials defined on the boundary $\partial\Omega$, where the integral kernels are given by directional derivatives of $\mathscr{G}$. By considering the power series expansions and addition formulae for the $\log(r)$ and $K_0(\lambda r)$ parts of $\mathscr{G}$ separately (see, for instance, [11]), any solution to (1) can be expressed using separation of variables in the interior of a disk by

$$u(r,\theta) = \sum_{n=-\infty}^{\infty} \left[\alpha_n r^{|n|} + \beta_n I_n(\lambda r)\right] e^{in\theta}. \tag{2}$$

In the exterior of a disk, assuming the solution is bounded, the general solution takes the form

$$u(r,\theta) = C_0 + C_1 K_0(\lambda r) + \sum_{\substack{n=-\infty \\ n\neq 0}}^{\infty} \left[\alpha_n r^{-|n|} + \beta_n K_n(\lambda r)\right] e^{in\theta}. \tag{3}$$

Unfortunately, using this representation naively for interior or exterior boundary value problems on a disk of radius R leads to numerical instabilities when the value λR is small. While this problem is of interest in its own right, such expansions play a role in more general domains when mulitpole and local expansions are used to represent outgoing and incoming fields in more general geometries, as explained below. Here, we propose a stabilized separation of variables approach based on a new class of special functions.

Remark 1 In the case of the bi-Helmholtz equation,

$$(\Delta - \lambda_1^2)(\Delta - \lambda_2^2) u = 0, \tag{4}$$

the separation of variables representation in the interior of a disk is given by

$$u(r,\theta) = \sum_{n=-\infty}^{\infty} \left[\alpha_n I_n(\lambda_1 r) + \beta_n I_n(\lambda_2 r)\right] e^{in\theta}. \tag{5}$$

In this setting, it is perhaps clearer that there are two dimensionless quantities involved: $\lambda_1 R$ and $\lambda_2 R$, with obvious ill-conditioning involved when $\lambda_1 \approx \lambda_2$.

The remainder of this paper is organized as follows. In sections 2, and 3, we provide some mathematical preliminaries, review the classical separation of variables approach to the modified biharmonic problem, and define new functions Q_n and P_n for stably representing solutions in the small λR regime. In section 4, we present numerical examples to illustrate the necessity for stabilization and to demonstrate the efficacy of our new functions. In the discussion of section 5, we outline how these functions can be used for stably solving (1) on more complex geometries with an accelerated integral equation method. Such methods depend on translation operators for series using the Q_n and P_n functions, for which we provide the necessary formulae. Appendix A includes some needed properties of Bessel and Laurent series.

2 Mathematical preliminaries

2.1 Notation

In the following, we use the "big O" notation to describe the order of the remaining terms in a power series. The expression $f(\varepsilon) = \mathcal{O}(g(\varepsilon))$ implies that there exist positive constants C and ε_0 such that

$$|f(\varepsilon)| \leq Cg(\varepsilon) \,, \tag{6}$$

when $0 < \varepsilon < \varepsilon_0$. As we are concerned with the asymptotic behavior with respect to two variables, we often write $f(\varepsilon, \delta) = \mathcal{O}(g(\varepsilon, \delta))$ which implies that there exist positive constants C, ε_0, and δ_0 such that

$$|f(\varepsilon, \delta)| \leq Cg(\varepsilon, \delta) \,, \tag{7}$$

when $0 < \varepsilon < \varepsilon_0$ and $0 < \delta < \delta_0$.

In section 5, we use the "big O" notation to describe computational cost. For this case, the expression $f(N) = \mathcal{O}(g(N))$ implies that there exist positive constants C and N_0 such that

$$|f(N)| \leq Cg(N) \,, \tag{8}$$

when $N > N_0$.

2.2 Condition numbers of 2×2 linear systems and diagonal scaling

In this section, we review some basic results from linear algebra. Consider an invertible linear system of the form

$$Ax = b \,. \tag{9}$$

The condition number $\kappa(A)$ of the matrix A describes the sensitivity of the problem of recovering x from b [26]. Suppose that an approximate solution x_0 is found such that

$$\frac{\|b - Ax_0\|_2}{\|b\|_2} = \varepsilon \,, \tag{10}$$

where $\|\cdot\|_2$ denotes the Euclidean norm. Let $\kappa(A) = \sigma_{\max}(A)/\sigma_{\min}(A)$, where $\sigma_{\max}(A)$ and $\sigma_{\min}(A)$ denote the maximum and minimum singular values of A. Then, x_0 satisfies

$$\frac{\|x - x_0\|_2}{\|x\|} \leq \kappa(A)\varepsilon \,. \tag{11}$$

Suppose that each column a_i of A represents some function from a basis and that x represents the coefficients which reconstruct b in that basis. In this case, the notion of the sensitivity of x to changes in b should be unaffected by scaling the columns of A. Let D be an invertible diagonal matrix and A, x, b, and x_0 be as above. We note that the residual is unaffected by scaling x_0 and A, i.e. that $\|b - Ax_0\|_2 = \|b - (AD)(D^{-1}x_0)\|_2$ but that the condition numbers of A and AD can be significantly different. To avoid this ambiguity, we quantify the sensitivity of recovering x from b in terms of the condition number of $\tilde{A} = AD$, where D is a diagonal matrix with $D_{ii} = 1/\|a_i\|_2$.

For 2×2 matrices, this is a natural normalization. It is straightforward to prove

Lemma 1 *Let A be a 2×2 matrix with columns a_i. If D is a diagonal matrix with $D_{ii} = 1/\|a_i\|_2$, then*

$$\kappa(AD) = \min_{v\in\mathbb{R}^2} \kappa(A\,\mathrm{diag}(v)) \,, \tag{12}$$

where $\mathrm{diag}(v)$ *denotes the diagonal matrix whose main diagonal is given by v.*

It is particularly simple to characterize the condition number of matrices with this scaling. We have

Lemma 2 *Let A be a 2×2 matrix with columns denoted by a_i. Suppose that $\|a_i\| = 1$. Then*

$$\kappa = \sqrt{\frac{1+c}{1-c}} \,, \tag{13}$$

where $c = |a_1^\intercal a_2|$ is the cosine of the angle between the two columns of A.

2.3 Separation of variables

Consider the modified biharmonic equation (1) where Ω is the disk of radius R centered at the origin. For given functions f and g, we prescribe Dirichlet boundary conditions on u, i.e.

$$u = f \text{ on } \partial\Omega \,, \tag{14}$$
$$\partial_n u = g \text{ on } \partial\Omega \,, \tag{15}$$

where ∂_n denotes the outward normal derivative. Other types of boundary conditions may be considered.

To take advantage of the simplicity of this geometry, we translate the problem to a polar coordinate system. Let (r,θ) denote the usual polar coordinates for the point $(x,y)\in\mathbb{R}^2$ as in the following change of variables

$$\begin{cases} x = r\cos(\theta) \\ y = r\sin(\theta) \end{cases} \leftrightarrow \begin{cases} r = \sqrt{x^2+y^2} \\ \theta = \arctan(y/x) \end{cases} \,, \tag{16}$$

with $\theta\in[-\pi,\pi)$. Then, the Laplacian is given by

$$\Delta = \partial_{rr} + \frac{1}{r}\partial_r + \frac{1}{r^2}\partial_{\theta\theta} \,. \tag{17}$$

Consider the boundary data as functions of the coordinate θ. For f and g sufficiently smooth, the Fourier series

$$f(R,\theta) = \sum_{n=-\infty}^{\infty} f_n e^{in\theta} \,, \tag{18}$$
$$g(R,\theta) = \sum_{n=-\infty}^{\infty} g_n e^{in\theta} \,, \tag{19}$$

converge uniformly in θ and the coefficients f_n and g_n are given by

$$f_n = \frac{1}{2\pi}\int_{-\pi}^{\pi} f(R,\theta)e^{-in\theta}\,d\theta\,, \tag{20}$$

$$g_n = \frac{1}{2\pi}\int_{-\pi}^{\pi} g(R,\theta)e^{-in\theta}\,d\theta\,. \tag{21}$$

Following standard practice [12,24], we seek a solution u of the form

$$u(r,\theta) = \sum_{n=-\infty}^{\infty} u_n(r)e^{in\theta}\,. \tag{22}$$

Plugging this form for u into (1), we obtain, after some simplification,

$$\sum_{n=-\infty}^{\infty}\left(\partial_{rr}+\frac{1}{r}\partial_r-\frac{n^2}{r^2}\right)\left(\partial_{rr}+\frac{1}{r}\partial_r-\frac{n^2}{r^2}-\lambda^2\right)u_n(r)e^{in\theta} = 0\,. \tag{23}$$

The above implies that the radial function $u_n(r)$ satisfies the following ordinary differential equation

$$\left(\frac{d^2}{dr^2}+\frac{1}{r}\frac{d}{dr}-\frac{n^2}{r^2}\right)\left(\frac{d^2}{dr^2}+\frac{1}{r}\frac{d}{dr}-\frac{n^2}{r^2}-\lambda^2\right)u_n(r) = 0\,, \tag{24}$$

subject to certain boundary or regularity conditions. For $n \neq -1,0,1$, we have

$$\begin{aligned} u_n(R) &= f_n\,, & u_n'(R) &= g_n\,,\\ u_n(0) &= 0\,, & u_n'(0) &= 0\,. \end{aligned} \tag{25}$$

For $n = 0$, we have

$$\begin{aligned} u_0(R) &= f_0\,, & u_0'(R) &= g_0\,,\\ u_0'(0) &= 0\,, & u_0'''(0) &= 0\,. \end{aligned} \tag{26}$$

Finally, for $n = -1,1$, we have

$$\begin{aligned} u_n(R) &= f_n\,, & u_n'(R) &= g_n\,,\\ u_n(0) &= 0\,, & u_n''(0) &= 0\,. \end{aligned} \tag{27}$$

The conditions at $r = 0$ are derived by assuming that u has four continuous derivatives at the origin.

It is well known [1,21] that equation (24) has the following four linearly independent solutions for $n \neq 0$: $r^{|n|}, r^{-|n|}, I_n(\lambda r), K_n(\lambda r)$, where I_n and K_n are the modified Bessel functions of the first and second kind, respectively. For $n = 0$, the functions $1, \log r, I_0(\lambda r), K_0(\lambda r)$ are linearly independent solutions. The regularity of the solution at zero eliminates $K_n(\lambda r), r^{-|n|}, \log r$ from the acceptable solution set. Therefore, the allowed functions u_n are linear combinations of the following form:

$$u_n(r) = \alpha_n r^{|n|} + \beta_n I_n(\lambda r)\,. \tag{28}$$

The boundary conditions for u_n determine α_n and β_n, with the conditions at $r = 0$ automatically satisfied. From the conditions at $r = R$, we obtain the following linear system for α_n and β_n

$$\begin{pmatrix} R^{|n|} & I_n(\lambda R) \\ |n|R^{|n|-1} & \dfrac{\lambda}{2}\left(I_{n-1}(\lambda R)+I_{n+1}(\lambda R)\right) \end{pmatrix} \begin{pmatrix} \alpha_n \\ \beta_n \end{pmatrix} = \begin{pmatrix} f_n \\ g_n \end{pmatrix} . \tag{29}$$

The determinant of the system in (29) is $\lambda R^{|n|} I_{n+1}(\lambda R)$, which is nonzero for positive R. Therefore, the coefficients α_n and β_n are determined by the boundary conditions and the above provides an algorithm for computing u.

In the exterior of a disk, the derivation is analogous to the above. For simplicity, we consider solutions of (1) which are bounded with derivatives that are $o(1/r)$ as r goes to infinity. This is sufficient for the solutions of the exterior problem to be unique; see, for example, Proposition 3.5 in [18]. The functions appropriate for the exterior of a disk are then $K_n(\lambda r)$ and $r^{-|n|}$. As in (29), we obtain a linear system for the expansion coefficients

$$\begin{pmatrix} R^{-|n|} & K_n(\lambda R) \\ -|n|R^{-|n|-1} & -\dfrac{\lambda}{2}\left(K_{n-1}(\lambda R)+K_{n+1}(\lambda R)\right) \end{pmatrix} \begin{pmatrix} \alpha_n \\ \beta_n \end{pmatrix} = \begin{pmatrix} f_n \\ g_n \end{pmatrix} . \tag{30}$$

The determinant of this system is $-\lambda K_{n-1}(\lambda R)/R^{|n|}$ so that it is invertible.

In order to make a numerical method out of the above, one simply truncates the Fourier series expansions at some finite N, i.e.

$$f(R,\theta) \approx \sum_{n=-N}^{N+1} f_n e^{in\theta} , \tag{31}$$

$$g(R,\theta) \approx \sum_{n=-N}^{N+1} g_n e^{in\theta} , \tag{32}$$

$$u(r,\theta) \approx \sum_{n=-N}^{N+1} u_n(r) e^{in\theta} . \tag{33}$$

The formulae (20) and (21) for the coefficients f_n and g_n can be approximated using the trapezoidal rule with $M = 2N+2$ equispaced points on $\partial\Omega$ and computed rapidly via the fast Fourier transform [10]. The rate of convergence (in N) depends on the smoothness of the boundary data f and g, with spectral convergence for analytic f and g.

3 Analysis of the separation of variables problem and new basis functions

The difficulty with the above procedure is in solving the linear systems (29), (30). In particular, for small λR, the columns of these system matrices are nearly linearly dependent, i.e., as λ goes to zero, the angle between the columns goes to zero (there is a similar effect for small R). As noted in section 2.2 this makes the problem of recovering the coefficients, α_n and β_n, from the data, f_n and g_n, unstable. In this section, we will investigate the nature of this ill-conditioning and derive new bases which are better conditioned.

We first fix some notation. For a pair of functions $(F(r), G(r))$, define the matrix $A(F,G,R)$ to be

$$A(F,G,R) = \begin{pmatrix} F(R) & G(R) \\ F'(R) & G'(R) \end{pmatrix} . \tag{34}$$

This is the form of the matrix that appears in the linear systems (29), (30) used to solve for the coefficients α_n and β_n. Let $\tilde{B}$ denote the matrix B with its columns normalized to unit length.

For the interior problem, the ill-conditioning of the basis $(r^{|n|}, I_n)$ results from the fact that the $I_n(\lambda r)$ and $r^{|n|}$ are very similar functions for small r; they have the same asymptotic behavior to leading order. The power series for $I_n(\lambda r)$ is given by

$$I_n(\lambda r) = \sum_{k=0}^{\infty} \frac{\left(\frac{\lambda r}{2}\right)^{2k+|n|}}{k!(k+|n|)!} = \frac{1}{2^{|n|}|n|!}(\lambda r)^{|n|} + \frac{1}{2^{|n|+2}(|n|+1)!}(\lambda r)^{|n|+2} + \cdots , \tag{35}$$

see [11, Ch. 10] for reference. By substituting this expression into $A(r^{|n|}, I_n, R)$, we obtain, for $n \neq 0$,

$$A(r^{|n|}, I_n, R) = \begin{pmatrix} R^{|n|} & R^{|n|} a_n(\lambda)(1+\mathscr{O}(\lambda^2 R^2)) \\ |n|R^{|n|-1} & |n|R^{|n|-1} a_n(\lambda)(1+\mathscr{O}(\lambda^2 R^2)) \end{pmatrix} , \tag{36}$$

where $a_n(\lambda) = \lambda^{|n|}/(2^{|n|}|n|!)$. We see that the columns of $\tilde{A}(r^{|n|}, I_n, R)$ are nearly co-linear in the limit as either λ or R goes to zero. The dependence on λ and R is not identical (this is wrapped up in the "big O" expressions); in the next section, we see that the condition number of the normalized matrix generally increases faster as R goes to zero than it does as λ goes to zero. For $n = 0$, we have the system

$$A(1, I_0, R) = \begin{pmatrix} 1 & 1+\mathscr{O}(\lambda^2 R^2) \\ 0 & \frac{1}{2}\lambda^2 R(1+\mathscr{O}(\lambda^2 R^2)) \end{pmatrix} , \tag{37}$$

so that the condition number increases faster as λ goes to zero in this case.

To alleviate this ill-conditioning, we construct basis functions which are more orthogonal in the small R and small λ limits. Let us define the functions $P_n(r)$ by

$$P_n(r) = I_n(\lambda r) - \left(\frac{\lambda r}{2}\right)^{|n|} \frac{1}{|n|!} , \tag{38}$$

deleting the first term in the power series for I_n. Note that, P_n is a solution of (24) because it is a linear combination of I_n and $r^{|n|}$. The matrix we obtain for the basis $(r^{|n|}, P_n)$ is

$$A(r^{|n|}, P_n, R) = \begin{pmatrix} R^{|n|} & R^{|n|+2} b_n(\lambda)(1+\mathscr{O}(\lambda^2 R^2)) \\ |n|R^{|n|-1} & (|n|+2)R^{|n|+1} b_n(\lambda)(1+\mathscr{O}(\lambda^2 R^2)) \end{pmatrix} , \tag{39}$$

where $b_n(\lambda) = \lambda^{|n|+2}/(2^{|n|+2}(|n|+1)!)$. As λ goes to zero, the columns of $\tilde{A}(r^{|n|}, P_n, R)$ do not converge to the same vector, as in the above. Further, as R goes to zero, the normalized columns do converge to the same limit but the effect is not as dramatic as for the pair $(r^{|n|}, I_n)$. The problem of recovering the coefficients is therefore more stable for the basis $(r^{|n|}, P_n)$, which we verify numerically in the next section.

Remark 2 It is simple to evaluate $P_n(r)$ stably. For small λr, the power series for I_n, with the first term omitted, may be used. For larger r, there is no fear of numerical cancellation and the formula (38) may be used directly, along with existing software for evaluating I_n. We choose the pair $(r^{|n|}, P_n)$ as opposed to (I_n, P_n) because P_n and $r^{|n|}$ have different asymptotic behavior for large r, whereas P_n and I_n both grow exponentially.

Remark 3 If the functions I_n and $r^{|n|}$ were used as a basis themselves, their asymptotic similarity in the small R regime would cause other numerical problems for a solution which behaves like P_n. To see this, note that for small r, the function $P_n(r)$ is $\mathcal{O}(r^{|n|+2})$, while the functions $I_n(r)$ and $r^{|n|}$ are $\mathcal{O}(r^{|n|})$. Therefore, there is significant numerical cancellation when evaluating $P_n(r)$ via the formula (38). We illustrate this effect in the next section.

A similar analysis applies to the exterior problem. The power series for $K_n(\lambda r)$ is given by

$$K_n(\lambda r) = \tfrac{1}{2}(\tfrac{1}{2}\lambda r)^{-|n|}\sum_{k=0}^{|n|-1}\frac{(|n|-k-1)!}{k!}(-\tfrac{1}{4}\lambda r^2)^k + (-1)^{|n|+1}\ln\left(\tfrac{1}{2}\lambda r\right) I_n(\lambda r) + (-1)^{|n|}\tfrac{1}{2}(\tfrac{1}{2}\lambda r)^{|n|}\sum_{k=0}^{\infty}\left(\psi(k+1)+\psi(|n|+k+1)\right)\frac{(\frac{1}{4}\lambda r^2)^k}{k!(|n|+k)!}\,, \tag{40}$$

where ψ denotes the digamma function (the digamma function is the logarithmic derivative of the gamma function, i.e. $\psi(z) = \Gamma'(z)/\Gamma(z)$). Substituting this expression into $A(r^{-|n|}, K_n, R)$, we obtain, for $n \neq 0$,

$$A(r^{-|n|}, K_n, R) = \begin{pmatrix} R^{-|n|} & R^{-|n|}c_n(\lambda)(1+\mathcal{O}(\lambda^2R^2)) \\ -|n|R^{-|n|-1} & -|n|R^{-|n|-1}c_n(\lambda)(1+\mathcal{O}(\lambda^2R^2)) \end{pmatrix}, \tag{41}$$

where $c_n(\lambda) = (|n|-1)!2^{|n|-1}\lambda^{-|n|}$. Again, after normalization, this linear system is ill-conditioned as either R or λ goes to zero because the normalized columns become nearly colinear. For the case $n = 0$, the basis $(1, K_0)$ results in the system

$$A(1, K_0, R) = \begin{pmatrix} 1 & -\gamma+\log(2)-\log(\lambda R)(1+\mathcal{O}(\lambda^2R^2)) \\ 0 & -\dfrac{1}{R}(1+\mathcal{O}(\lambda^2R^2|\log(\lambda R)|)) \end{pmatrix}, \tag{42}$$

which is actually well conditioned, after normalization, for small λ and R. For certain exterior problems, the basis $(\log r, K_0)$ is more appropriate. In this case, we have

$$A(\log r, K_0, R) = \begin{pmatrix} \log R & -\gamma+\log(2)-\log(\lambda R)(1+\mathcal{O}(\lambda^2R^2)) \\ \dfrac{1}{R} & -\dfrac{1}{R}(1+\mathcal{O}(\lambda^2R^2|\log(\lambda R)|)) \end{pmatrix}. \tag{43}$$

After normalization, this system is generally well-conditioned as λ goes to zero. As R goes to zero, however, the two columns become nearly colinear and the normalized matrix is ill-conditioned. Regardless of these special cases, the instability for the $n \neq 0$ coefficients will negatively affect the separation of variables approach.

To avoid this instability, we can define new functions Q_n for $n \neq 0$ as

$$Q_n(r) = K_n(\lambda r) - \frac{2^{|n|-1}(|n|-1)!}{\lambda^{|n|}r^{|n|}}\,. \tag{44}$$

The function Q_n has a different leading order term from K_n as λ and r go to zero but is still a solution of (24) as it is a linear combination of K_n and $r^{-|n|}$. As noted above, the system (30) is well conditioned for the functions 1 and $K_0(\lambda r)$. Therefore, the naïve approach works for the zero mode, for the particular conditions we have set at infinity. It is convenient, however, to define Q_0 as

$$Q_0(r) = K_0(\lambda r) + \log(r)\,. \tag{45}$$

This function is closely related to the Green's function for the modified biharmonic equation.

As before, the ill-conditioning of the coefficient recovery problem (29) is improved using the pair of functions (Q_n, K_n) as the basis. For $|n| > 2$, we obtain a system of the form

$$A(Q_n, K_n, R) = \begin{pmatrix} R^{-|n|+2} d_n(\lambda)(1+\mathscr{O}(\lambda^2 R^2)) & R^{-|n|} c_n(\lambda)(1+\mathscr{O}(\lambda^2 R^2)) \\ (-|n|+2)R^{-|n|+1} d_n(\lambda)(1+\mathscr{O}(\lambda^2 R^2)) & -|n| R^{-|n|-1} c_n(\lambda)(1+\mathscr{O}(\lambda^2 R^2)) \end{pmatrix}, \quad (46)$$

where $d_n(\lambda) = -2^{|n|-3}(|n|-2)!\lambda^{-|n|+2}$. As λ goes to zero, the normalized columns of this system matrix do not converge to the same vector, as in the above. Further, as R goes to zero, the columns do converge but the effect is not as dramatic as for the pair $(r^{-|n|}, K_n)$. The problem of recovering the coefficients is therefore more stable for the basis (Q_n, K_n) than it is for the basis $(r^{-|n|}, K_n)$, which we verify numerically in the next section.

Remark 4 It is simple to evaluate $Q_n(r)$ stably. For small r, the power series for K_n, with the first term omitted, may be used. For larger r, there is no fear of numerical cancellation and the formula (44) may be used directly, along with existing software for evaluating K_n. We choose the pair (Q_n, K_n) as opposed to $(r^{-|n|}, Q_n)$ because Q_n and K_n have different asymptotic behavior for large r.

Remark 5 If the functions K_n and $r^{-|n|}$ are used as a basis, their asymptotic similarity in the small R regime will cause other numerical problems for a solution with terms like Q_n. Suppose that K_n and $r^{-|n|}$ are used to evaluate Q_n. For small r, the function $Q_n(r)$ is $\mathscr{O}(r^{-|n|+2})$, while the functions $K_n(r)$ and $r^{-|n|}$ are $\mathscr{O}(r^{-|n|})$. Therefore, there is significant numerical cancellation when evaluating $Q_n(r)$ via the formula (44). We demonstrate this effect as well in the next section.

Before proceeding to the numerical experiments, we briefly describe the edge cases, i.e. the matrices for $|n| \leq 2$. When $|n| = 2$, the pair (Q_n, K_n) results in a linear system of the form

$$A(Q_2, K_2, R) \begin{pmatrix} -\frac{1}{2} + \mathscr{O}(R^2\lambda^2 |\log(\lambda R)|) & \frac{2}{\lambda^2 R^2} + \mathscr{O}(1) \\ -\frac{1}{4}\lambda^2 R \log(\lambda R) + \mathscr{O}(\lambda^2 R) & -\frac{4}{\lambda^2 R^3} + \mathscr{O}(\lambda^2 R |\log(\lambda R)|) \end{pmatrix}. \quad (47)$$

The columns of this matrix, after normalization, do not become colinear as either λ or R tends to zero. For the case that $|n| = 1$, the pair (Q_n, K_n) results in a linear system of the form

$$A(Q_1, K_1, R) = \begin{pmatrix} \frac{1}{2}\lambda R \log(\lambda R) + \mathscr{O}(\lambda R) & \frac{1}{\lambda R} + \mathscr{O}(\lambda R |\log(\lambda R)|) \\ \frac{1}{2}\lambda \log(\lambda R) + (\lambda + R^2) & -\frac{1}{\lambda R^2} + \mathscr{O}(\lambda |\log(\lambda R)|) \end{pmatrix}, \quad (48)$$

which has nearly colinear columns after normalization as R goes to zero. The normalized columns are not colinear in the limit as λ goes to zero. Finally, for the case $n = 0$, the pair (Q_n, K_n) results in a linear system of the form

$$\begin{pmatrix} -\log(\lambda/2) - \gamma + \mathscr{O}(\lambda^2 R^2 |\log(\lambda R)| & -\log(\lambda R/2) - \gamma + \mathscr{O}(\lambda^2 R^2 |\log(\lambda R)| \\ -\frac{1}{2}\lambda^2 R \log(\lambda R) + \mathscr{O}(\lambda^2 R) & -\frac{1}{R} + \mathscr{O}(\lambda^2 R |\log(\lambda R)|) \end{pmatrix} \begin{pmatrix} \alpha_n \\ \beta_n \end{pmatrix} = \begin{pmatrix} f_n \\ g_n \end{pmatrix}. \quad (49)$$

As λ goes to zero, the columns of this matrix slowly become colinear after normalization. As R goes to zero, the normalized columns do not become colinear.

4 Numerical tests

In this section we present some numerical experiments which reinforce the ideas of the previous section. The source code used for these calculations is available online [3]. The Bessel functions were evaluated using routines from FMMLIB2D [14]. Discrete Fourier transforms were computed using the FFTPACK [25]. To compute condition numbers, we used the singular value decomposition routine from EISPACK [13]. All code was written in Fortran using double precision arithmetic and compiled with the gfortran compiler on Linux.

4.1 Condition numbers

For the first test, we verify the analytical observations about the condition numbers of the matrices described in the previous section. For a pair of functions $(F(r),G(r))$, define the matrix $A(F,G,R)$ as in (34). Let $\tilde{B}$ denote the matrix B with its columns normalized to unit length. We compute the condition number of $\tilde{A}(F,G,R)$ where (F,G) is taken to be each of the bases $(r^{|n|},I_n(\lambda r))$, $(r^{|n|},P_n(\lambda r))$, $(r^{-|n|},K_n(\lambda r))$, and $(Q_n(\lambda r),K_n(\lambda r))$ for a range of values of n, λ, and R. To observe the effect of changing the radius of the domain, we run experiments with λ fixed (at $\lambda = 0.5$) and, for each j from -24 to 8, ten values of R drawn uniformly at random from the interval $[2^j,2^{j+1}]$. Likewise, to observe the effect of changing the parameter λ, we run experiments with R fixed (at $R = 0.5$) and, for each j from -24 to 8, ten values of λ drawn uniformly at random from the interval $[2^j,2^{j+1}]$. In order to compare these, we plot the condition number as a function of the product λR.

In fig. 1, we plot the results for the interior problem. The new basis $(r^{|n|},P_n)$ has smaller condition numbers than the basis $(r^{|n|},I_n)$, as either λ or R goes to zero. In the limit as λ goes to zero, we see that the condition number remains roughly constant for $(r^{|n|},P_n)$. In the limit as R goes to zero, there is some growth in the condition number for $(r^{|n|},P_n)$, except for the case $n = 0$, where it again remains roughly constant. For the basis $(r^{|n|},I_n)$, the condition number grows as either λ or R tends to zero and is larger than for the basis $(r^{|n|},P_n)$. The condition number tends to grow faster as R goes to zero compared to the growth as λ goes to zero, except for the case $n = 0$, in which we see the opposite trend. These results agree well with the analysis of section 3.

In fig. 2, we plot the results for the exterior problem. The new basis (Q_n,K_n) generally has smaller condition numbers than the basis $(r^{-|n|},K_n)$, as either λ or R goes to zero. In the limit as λ goes to zero, we see that the condition number remains roughly constant for (Q_n,K_n). In the limit as R goes to zero, there is some growth in the condition number for (Q_n,K_n), except for the cases $n = 0$ and $n = 2$, where it again remains roughly constant. For the basis $(r^{-|n|},K_n)$, the condition number grows faster as R goes to zero compared to the growth as λ goes to zero. The condition number for the basis $(r^{-|n|},K_n)$ does grow as λ tends to zero, except in the case that $n = 0$, for which the condition number remains roughly constant. Note that for $n = 0$ we have used the basis $(\log(r),K_0)$ as this set of functions is required to represent the synthetic solution used for the error analysis of the next section. Again, these results agree well with the analysis of section 3.

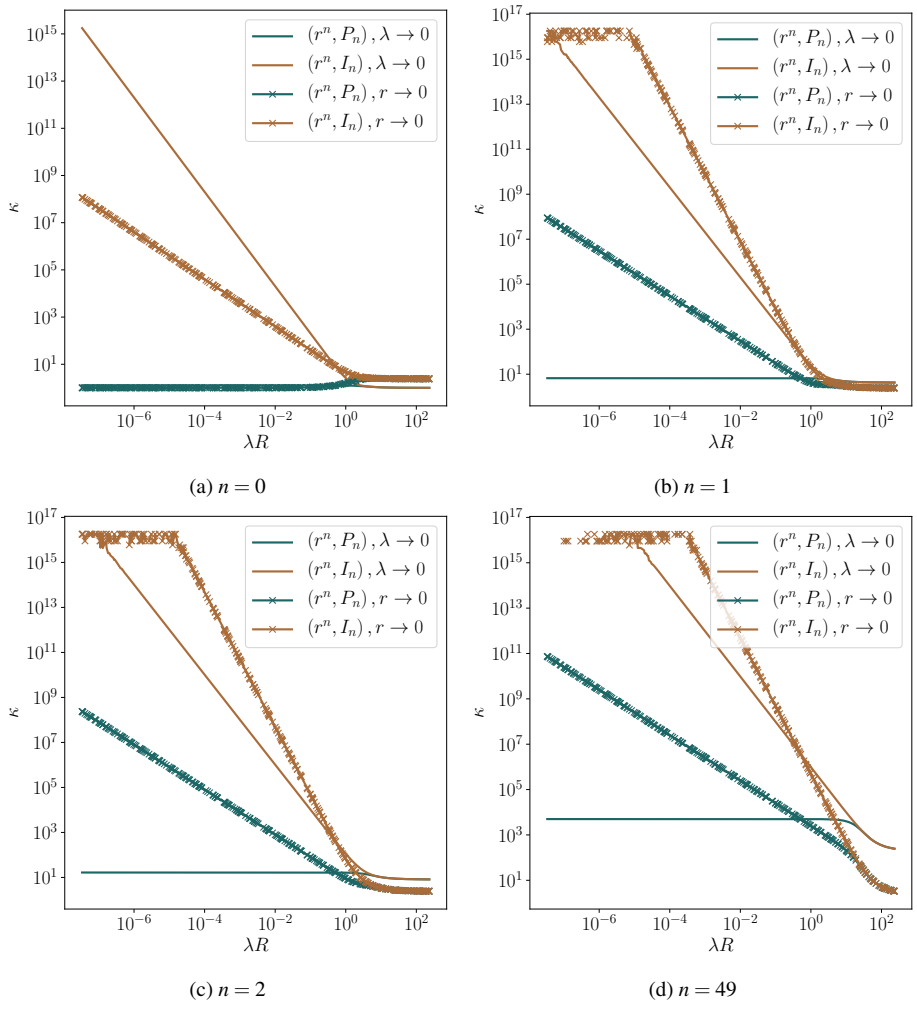

(a) $n = 0$ (b) $n = 1$

(c) $n = 2$ (d) $n = 49$

Fig. 1: We plot the condition number of the linear system (34) (after scaling the columns) for various values of n as a function of λR.

Remark 6 In figs. 1 and 2, we observe two distinct behaviors when λ tends to zero for a fixed R and vice-versa. This phenomenon is related to the two relevant scales of the bi-Helmholtz kernel noted in remark 1, though more extreme: whereas the bi-Helmholtz operator is the composition of two operators with their own dimensionless parameters, the modified biharmonic operator is the composition of two operators, one of which is scale-invariant and the other is not. In the next set of experiments, we see that, in many applications, there is only one relevant scaling for the modified biharmonic equation.

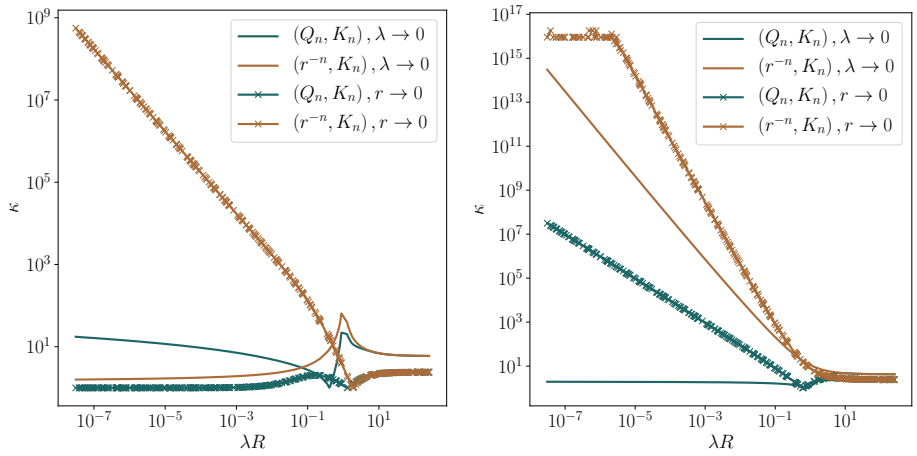

(a) $n = 0$ (b) $n = 1$

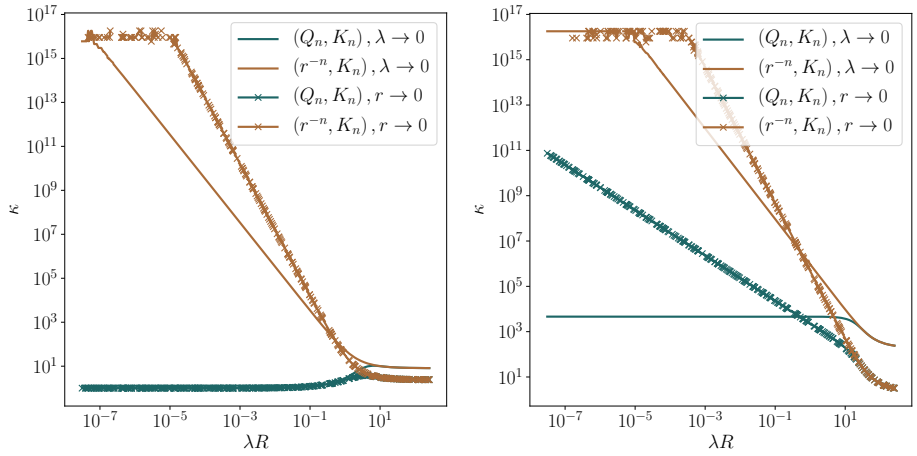

(c) $n = 2$ (d) $n = 49$

Fig. 2: We plot the condition number of the linear system (34) (after scaling the columns) for various values of n as a function of λR.

4.2 Error plots for known solution

In order to test the practical effect of the ill-conditioning seen in the last section, we use the separation of variables procedure to solve the modified biharmonic equation (1) on a disk with boundary conditions corresponding to a known solution. We construct this solution using the free-space Green's function for the modified biharmonic equation, which is defined as

$$\mathscr{G}(\mathbf{x},\mathbf{y}) = -\frac{1}{2\pi\lambda^2}\left(K_0(\lambda\rho) + \log(\rho)\right) , \tag{50}$$

where $\rho = \sqrt{(x_1-y_1)^2+(x_2-y_2)^2}$. The solution is then set to be

$$u(\mathbf{x};\lambda) = \sum_{j=1}^{n_s} \lambda^2 c_j \mathscr{G}(\mathbf{x},\mathbf{s}_j) + \lambda d_j \partial_{v_{j,1}} \mathscr{G}(\mathbf{x},\mathbf{s}_j) + q_j \partial_{v_{j,2} v_{j,3}} \mathscr{G}(\mathbf{x},\mathbf{s}_j), \tag{51}$$

where the $\mathbf{s}_j$ are $n_s = 100$ "source" points located outside of the domain, the c_j are drawn uniformly randomly from $[-1,1]$, the d_j and q_j are drawn uniformly randomly from $[0,1]$, and the vectors $v_{j,1}, v_{j,2}, v_{j,3}$ are defined by drawing the entries uniformly at random from $[-1/2,1/2]$ and normalizing. We note that the λ^2 and λ scales in front of the c_j and d_j are included to ensure that these terms are of roughly the same size as λ shrinks.

To implement separation of variables, we discretize the boundary with $M = 100$ points, so that $N = 49$ (the separation of variables expansion runs from $-N$ to $N+1$ as in section 2.3). We evaluate the function $u(\mathbf{x};\lambda)$ and its normal derivative on the boundary of the disk and compute their Fourier coefficients, i.e. the values f_n and g_n as in (20), (21), using the FFT. We then solve for the coefficients α_n and β_n by inverting the linear system

$$\begin{pmatrix} F_n(R) & G_n(R) \\ F_n'(R) & G_n'(R) \end{pmatrix} \begin{pmatrix} \alpha_n \\ \beta_n \end{pmatrix} = \begin{pmatrix} f_n \\ g_n \end{pmatrix}, \tag{52}$$

where $(F_n(r), G_n(r))$ is an appropriate pair of basis functions. For the sake of stability, the inversion is performed using Gaussian elimination with complete pivoting. Once the coefficients α_n and β_n have been computed, the approximate solution $\hat{u}$ can be evaluated using the formula

$$\hat{u}(\mathbf{x}) = \sum_{n=-N}^{N+1} (\alpha_n F_n(\rho) + \beta_n G_n(\rho)) e^{in\theta}, \tag{53}$$

where (ρ,θ) are the polar coordinates of $\mathbf{x}$. The derivatives of $\hat{u}$ can be obtained by differentiating this expression.

To measure the performance of the separation of variables method, we evaluate $\hat{u}$ and its first and second derivatives at $n_t = 100$ "target" points $\mathbf{t}_i$ located inside the domain. We then define three error measures

$$E_u = \sqrt{\frac{\sum_{i=1}^{n_t} (u(\mathbf{t}_i;\lambda) - \hat{u}(\mathbf{t}_i))^2}{\sum_{i=1}^{n_t} u(\mathbf{t}_i;\lambda)^2}}, \tag{54}$$

$$E_g = \sqrt{\frac{\sum_{i=1}^{n_t} (u_x(\mathbf{t}_i;\lambda) - \hat{u}_x(\mathbf{t}_i))^2 + (u_y(\mathbf{t}_i;\lambda) - \hat{u}_y(\mathbf{t}_i))^2}{\sum_{i=1}^{n_t} u_x(\mathbf{t}_i;\lambda)^2 + u_y(\mathbf{t}_i;\lambda)^2}}, \tag{55}$$

$$E_h = \sqrt{\frac{\sum_{i=1}^{n_t} (u_{xx}(\mathbf{t}_i;\lambda) - \hat{u}_{xx}(\mathbf{t}_i))^2 + (u_{xy}(\mathbf{t}_i;\lambda) - \hat{u}_{xy}(\mathbf{t}_i))^2 + (u_{yy}(\mathbf{t}_i;\lambda) - \hat{u}_{yy}(\mathbf{t}_i))^2}{\sum_{i=1}^{n_t} u_{xx}(\mathbf{t}_i;\lambda)^2 + u_{xy}(\mathbf{t}_i;\lambda)^2 + u_{yy}(\mathbf{t}_i;\lambda)^2}}, \tag{56}$$

which represent the relative error in the solution, gradient, and Hessian, respectively.

As in the previous section, we run the tests with a variety of values for the radius of the disk R and the parameter λ. To observe the effect of changing the radius of the domain, we run experiments with λ fixed (at $\lambda = 0.5$) and, for each j from -24 to 8, ten values of R drawn uniformly at random from the interval $[2^j, 2^{j+1}]$. Likewise, to observe the effect of changing the parameter λ, we run experiments with R fixed (at $R = 0.5$) and, for each j from -24 to 8, ten values of λ drawn uniformly at random from the interval $[2^j, 2^{j+1}]$. In order to compare these, we plot the error measures E_u, E_g, and E_h as functions of the product λR.

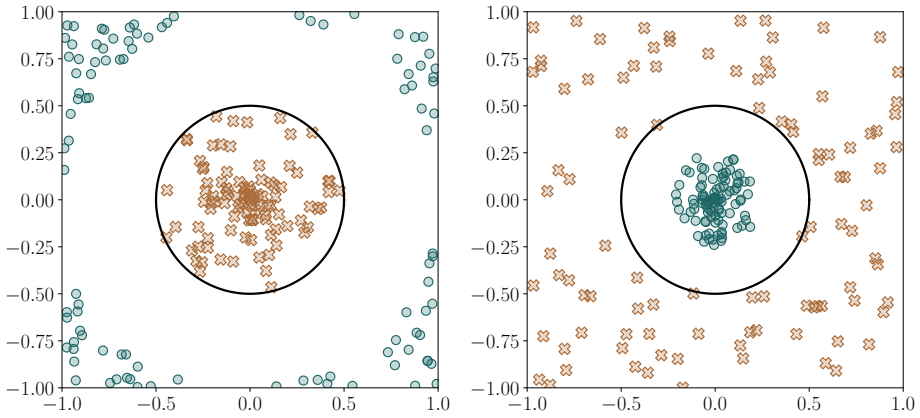

(a) Interior problem geometry (b) Exterior problem geometry

Fig. 3: Sample geometries for the interior and exterior problems with $R = 0.5$. The targets are marked by crosses and the sources by circles.

For the interior problem, the source points are drawn uniformly at random from the box $[-2R,2R]\times[-2R,2R]$ outside of the disk of radius $2R$. With this placement of source points, the length $N = 49$ expansion for $\hat{u}$ should be sufficient for approximately machine precision accuracy, based on standard multipole estimates [16,9]. The target points are drawn uniformly at random from the disk of radius R. We plot a sample arrangement of the source and target points for the interior problem in fig. 3a.

Similarly, for the exterior problem, the source points are drawn uniformly at random from the disk of radius $R/2$. This placement is again chosen so that the length $N = 49$ expansion for $\hat{u}$ is sufficient for approximately machine precision accuracy. The target points are drawn uniformly at random from the box $[-2R,2R]\times[-2R,2R]$ outside of the disk of radius R. We plot a sample arrangement of the source and target points for the exterior problem in fig. 3b.

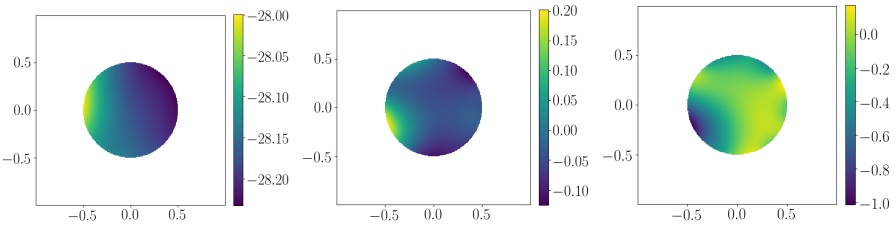

(a) u (b) u_x (c) u_{xy}

Fig. 4: Heatmaps of the exact solution u and select derivatives for the interior problem with $R = 0.5$ and $\lambda = 2^{-24}$.

In figs. 4 and 5 we plot a sample exact solution u and some select derivatives for the interior and exterior problems, respectively. For the following error plots, we consider the

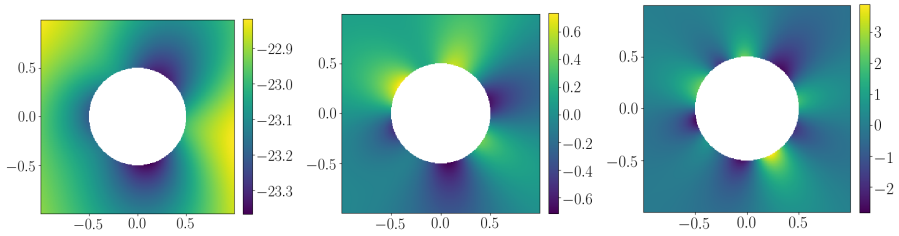

(a) u (b) u_x (c) u_{xy}

Fig. 5: Heatmaps of the exact solution u and select derivatives for the exterior problem with $R = 0.5$ and $\lambda = 2^{-24}$.

error in approximating these solutions using the bases we have discussed above as well as using what we call the "exact difference". We include the exact difference figure to emphasize that it is not only the ability to recover α_n and β_n that causes trouble using the naïve bases. Because u is defined in terms of the Green's function $\mathscr{G}$, which is simply a scaled sum of the Green's functions for the Laplace and modified Helmholtz equations, we could reasonably evaluate u by evaluating these parts separately and combining them in the end. Let u_L and u_H be defined as

$$u_L(\mathbf{x};\lambda) = \frac{1}{2\pi\lambda^2}\sum_{j=1}^{n_s} \lambda^2 c_j \log\|\mathbf{x}-\mathbf{s}_j\|_2 + \lambda d_j \partial_{v_{j,1}} \log\|\mathbf{x}-\mathbf{s}_j\|_2 + q_j \partial_{v_{j,2}v_{j,3}} \log\|\mathbf{x}-\mathbf{s}_j\|_2 \tag{57}$$

and

$$u_H(\mathbf{x};\lambda) = -\frac{1}{2\pi\lambda^2}\sum_{j=1}^{n_s} \lambda^2 c_j K_0(\lambda\|\mathbf{x}-\mathbf{s}_j\|_2) + \lambda d_j \partial_{v_{j,1}} K_0(\lambda\|\mathbf{x}-\mathbf{s}_j\|_2) + q_j \partial_{v_{j,2}v_{j,3}} K_0(\lambda\|\mathbf{x}-\mathbf{s}_j\|_2)\,. \tag{58}$$

The "exact difference" error below is the error in evaluating u as the difference $u_H - u_L$ in floating point arithmetic.

In fig. 6, we plot the error measures as functions of λR for both the limit as R goes to zero with λ fixed and vice-versa, for the interior problem. The behavior of the two limits is similar, in contrast with the condition numbers of the previous section. This is an indication that λR is the relevant figure for applications. We see that the new basis $(r^{|n|}, P_n)$ is able to achieve high accuracy, even as λR tends to zero. We note that E_u is around machine precision, and there is some precision loss for the errors of the derivatives, E_g and E_h. When using the naïve basis, $(r^{|n|}, I_n)$, on the other hand, there is significant loss of accuracy as λR goes to zero. The error in evaluating the exact difference between the harmonic and modified Helmholtz parts agrees well with the naïve basis $(r^{|n|}, I_n)$ in the small λR limit. This error for the exact difference shows that there is a fundamental problem in using the basis $(r^{|n|}, I_n)$ to represent such solutions. For large λR, the exact difference is capable of near machine precision in even the derivatives, as the procedure does not really involve numerical differentiation. We see similar behavior for the exterior problem in fig. 7.

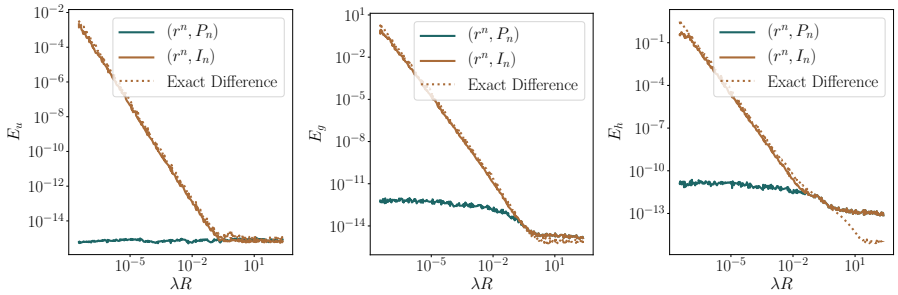

(a) E_u as λ goes to zero. (b) E_g as λ goes to zero. (c) E_h as λ goes to zero.

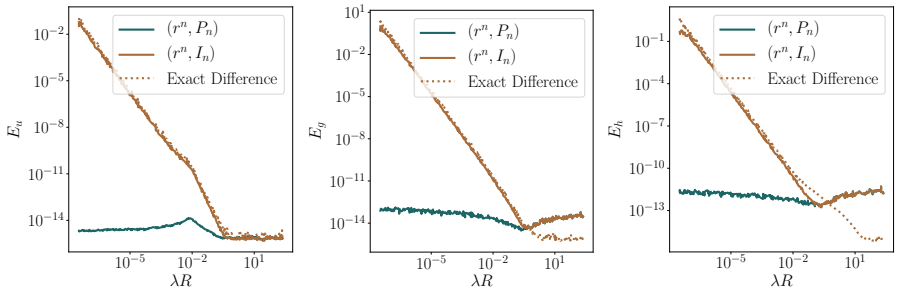

(d) E_u as R goes to zero. (e) E_g as R goes to zero. (f) E_h as R goes to zero.

Fig. 6: Interior problem. In the top row, we plot the error measures as functions of λR for $R = 0.5$ as λ goes to zero. In the bottom row, we plot the error measures as functions of λR for $\lambda = 0.5$ as R goes to zero.

5 Discussion

In the preceding, we have shown that the new bases $(r^{|n|}, P_n)$ and (Q_n, K_n) offer significant advantages over the naïve approach when solving the modified biharmonic equation on a disk. We now show how these functions can be used to efficiently solve the modified biharmonic equation (1) on more complex geometries.

5.1 Integral equations

Because (1) is a homogeneous, fourth order equation, it is well suited to solution using an integral equation formulation. We do not attempt a review of the literature here but point to [7, 15, 8, 4, 18] for some representative examples. In an integral equation method, the solution on any domain Ω is represented by a layer potential with unknown densities defined on the boundary $\partial\Omega$, i.e.

$$u(\mathbf{x}) = \int_{\partial\Omega} K_1(\mathbf{x},\mathbf{y})\sigma_1(\mathbf{y}) + K_2(\mathbf{x},\mathbf{y})\sigma_2(\mathbf{y})\, dS(\mathbf{y}) \,, \tag{59}$$

where the kernels K_1 and K_2 are typically defined in terms of directional derivatives of the free-space Green's function $\mathscr{G}$. For example, in [18], the kernels are $K_1 = -\mathscr{G}_{\nu\nu} + \mathscr{G}_{\tau\tau}$ and $K_2 = -2\mathscr{G}_{\nu\nu\nu} + 3(\Delta - \lambda^2)G_\nu + 2\lambda^2\mathscr{G}_\nu$, where ν and τ represent the normal and tangential directions at $\mathbf{y}$, respectively.

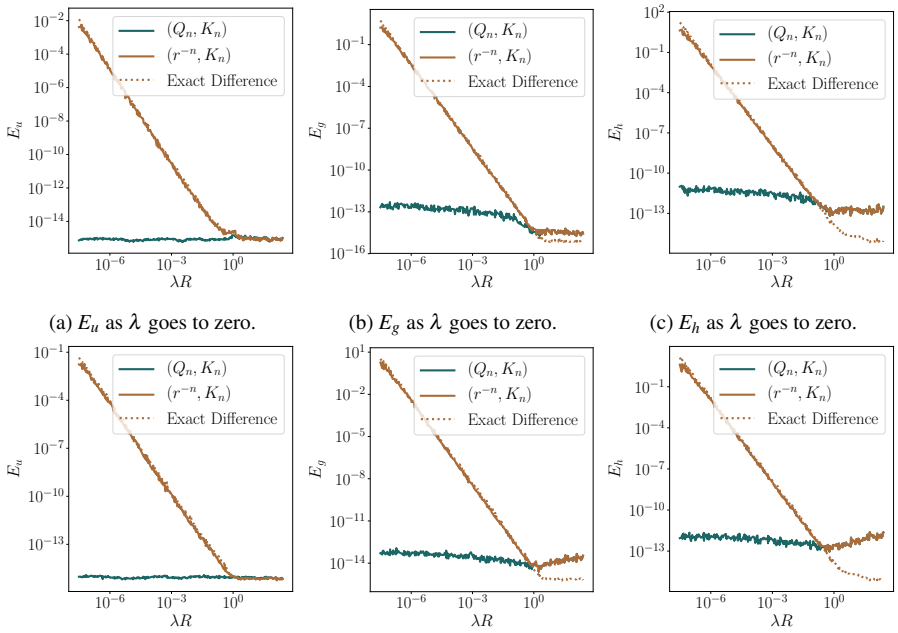

(a) E_u as λ goes to zero. (b) E_g as λ goes to zero. (c) E_h as λ goes to zero.

(d) E_u as R goes to zero. (e) E_g as R goes to zero. (f) E_h as R goes to zero.

Fig. 7: Exterior problem. In the top row, we plot the error measures as functions of λR for $R = 0.5$ as λ goes to zero. In the bottom row, we plot the error measures as functions of λR for $\lambda = 0.5$ as R goes to zero.

Continuing the example, the authors of [18] then impose gradient boundary conditions on u, i.e. they set $\partial_{\nu_x} u = f$ and $\partial_{\tau_x} u = g$ for some functions f and g defined on the boundary, where ν_x and τ_x denote the normal and tangential directions at a point $\mathbf{x}$ on the boundary. These boundary conditions are of physical interest because they correspond to "no-slip" boundary conditions for a stream function representation of a fluid flow. Plugging the form (59) into the boundary conditions, we obtain the integral equation

$$\begin{pmatrix} D_{11}(\mathbf{x}) & D_{12}(\mathbf{x}) \\ 0 & D_{22}(\mathbf{x}) \end{pmatrix} \begin{pmatrix} \sigma_1(\mathbf{x}) \\ \sigma_2(\mathbf{x}) \end{pmatrix} + \int_{\partial\Omega} \begin{pmatrix} K_{11}(\mathbf{x},\mathbf{y}) & K_{12}(\mathbf{x},\mathbf{y}) \\ K_{21}(\mathbf{x},\mathbf{y}) & K_{22}(\mathbf{x},\mathbf{y}) \end{pmatrix} \begin{pmatrix} \sigma_1(\mathbf{y}) \\ \sigma_2(\mathbf{y}) \end{pmatrix} dS(\mathbf{y}) = \begin{pmatrix} f(\mathbf{x}) \\ g(\mathbf{x}) \end{pmatrix}, \tag{60}$$

where $K_{11} = \partial_{\nu_x} K_1$, $K_{12} = \partial_{\nu_x} K_2$, $K_{21} = \partial_{\tau_x} K_1$, and $K_{22} = \partial_{\tau_x} K_2$. See [18] for details, including a simple preconditioner for turning (60) into a well-conditioned second kind integral equation and explicit formulae for the kernels K_{ij}.

In a Nyström discretization of the integral equation (60), the solution is represented by its values at points on the curve $\partial\Omega$ which are used for an integration rule. The basis of a Nyström method is then a numerical quadrature of the integral operator on the curve $\partial\Omega$. Typically, different integration rules are required for smooth, weakly singular, and singular integral kernels. Fortunately, a number of quadrature rules are available for handling these singularities with high order accuracy [2, 19, 5, 17].

Let $\mathbf{x}_i$ denote the points on $\partial\Omega$ of the Nyström discretization, $\sigma_{1i} = \sigma_1(\mathbf{x}_i)$, $\sigma_{2i} = \sigma_2(\mathbf{x}_i)$, $f_i = f(\mathbf{x}_i)$, and $g_i = g(\mathbf{x}_i)$. In a slight abuse of notation, the quadrature rule provides weights w_{ij} such that

$$\begin{pmatrix} D_{11}(\mathbf{x}_i) & D_{12}(\mathbf{x}_i) \\ 0 & D_{22}(\mathbf{x}_i) \end{pmatrix} \begin{pmatrix} \sigma_{1i} \\ \sigma_{2i} \end{pmatrix} + \sum_j w_{ij} \begin{pmatrix} K_{11}(\mathbf{x}_i,\mathbf{x}_j) & K_{12}(\mathbf{x}_i,\mathbf{x}_j) \\ K_{21}(\mathbf{x}_i,\mathbf{x}_j) & K_{22}(\mathbf{x}_i,\mathbf{x}_j) \end{pmatrix} \begin{pmatrix} \sigma_{1j} \\ \sigma_{2j} \end{pmatrix} = \begin{pmatrix} f_i \\ g_i \end{pmatrix}, \tag{61}$$

is an accurate approximation of the original integral equation at each point $\mathbf{x}_i$. The above is an abuse of notation because the kernels are not often defined when $\mathbf{x} = \mathbf{y}$, so that the formula is in general a function of the kernel and the boundary. A key feature of these integral rules is that the weight w_{ij} is typically a function of j alone for points $\mathbf{x}_i$ and $\mathbf{x}_j$ which are sufficiently far apart. Therefore, much of the sum (61) is of a form which is amenable to a fast multipole method (FMM) — which we outline in the next section — so that the operator on the left-hand-side of (61) may be applied rapidly. Combined with an iterative solver such as GMRES [23], this provides a fast solution method for the densities σ_1 and σ_2. The FMM can also be utilized to efficiently evaluate the formula for u, i.e. (59), at points inside the domain [17,20,22].

5.2 Fast sums

Let $\mathbf{x}_i$ be a set of N points in space. Suppose that we would like to evaluate the sum

$$u(\mathbf{x}_i) = \sum_{j\neq i}^{N} \lambda^2 c_j \mathscr{G}(\mathbf{x}_i,\mathbf{x}_j) + \lambda d_j \partial_{v_{j,1}} \mathscr{G}(\mathbf{x}_i,\mathbf{x}_j) + q_j \partial_{v_{j,2}v_{j,3}} \mathscr{G}(\mathbf{x}_i,\mathbf{x}_j), \tag{62}$$

for each $\mathbf{x}_i$ efficiently. Direct evaluation would be an $\mathscr{O}(N^2)$ calculation. When performing the analogous sum with the Laplace Green's function, the original FMM [16,6] provides a stable $\mathscr{O}(N)$ algorithm. We do not seek to review the details of an FMM algorithm here, but we note that such a method depends on a few key parts: a formula for representing the sum due to a localized subset of the points (a multipole expansion), a formula for representing the sum due to points outside of a disk (a local expansion), formulae for translating between these representations (translation operators), and a hierarchical organization of the points in space. For details, see [16,6].

Following the results of the previous section, we see that an expansion in terms of the functions (Q_n, K_n) provides a stable representation for the sum due to points contained inside a disk when evaluated at points sufficiently far from that disk. Similarly, an expansion in terms of the functions $(r^{|n|}, P_n)$ can be used to stably represent the sum due to points located sufficiently far outside of a disk. These are then our multipole and local expansions, respectively.

Starting with the formulae for translating multipole and local expansions for the Laplace and modified Helmholtz Green's functions, which are included in appendix A, it is straightforward to derive translation operators for the (Q_n, K_n) and $(r^{|n|}, P_n)$ expansions. The center of a (Q_n, K_n) multipole expansion can be shifted using the following formula:

Lemma 3 *Suppose that*

$$\phi(\mathbf{x}) = \sum_{l=-\infty}^{\infty} \left(a_l Q_l(\rho') + b_l K_l(\lambda\rho')\right) e^{il\theta'}, \tag{63}$$

where (ρ', θ') *are the polar coordinates of* $\mathbf{x}$ *with respect to the point* $\mathbf{x}_0$*, is a multipole expansion of the potential due to a charge density which is contained inside the disk of radius* R *about* $\mathbf{x}_0$*. Let* (ρ_0, θ_0) *be the polar coordinates of* $\mathbf{x}_0$ *with respect to the origin. Then, for* $\mathbf{x}$ *outside the disk of radius* $R+\rho_0$*, we have*

$$\phi(\mathbf{x}) = \sum_{l=-\infty}^{\infty} \left(c_l Q_l(\rho) + d_l K_l(\lambda\rho)\right) e^{il\theta} \,, \tag{64}$$

where (ρ, θ) *are the coordinates of* $\mathbf{x}$ *with respect to the origin. We have that* $c_0 = a_0$ *and*

$$\begin{aligned} d_0 = &\sum_{m=-\infty}^{-1} (a_m + b_m) I_{-m}(\lambda\rho_0) e^{-i(l-m)\theta_0} + a_0 P_0(\lambda\rho_0) + b_0 I_0(\lambda\rho_0) \\ &+ \sum_{m=1}^{\infty} (a_m + b_m) I_{-m}(\lambda\rho_0) e^{-i(l-m)\theta_0} \,. \end{aligned} \tag{65}$$

For $l > 0$ *the translated coefficients are given by*

$$c_l = \sum_{m=0}^{l} a_m \left(\frac{\lambda\rho_0}{2}\right)^{l-m} \frac{e^{-i(l-m)\theta_0}}{(l-m)!} \tag{66}$$

and

$$\begin{aligned} d_l = &\sum_{m=-\infty}^{-1} (a_m + b_m) I_{l-m}(\lambda\rho_0) e^{-i(l-m)\theta_0} \\ &+ \sum_{m=0}^{l} (a_m P_{l-m}(\rho_0) + b_m I_{l-m}(\lambda\rho_0)) e^{-i(l-m)\theta_0} \\ &+ \sum_{m=l+1}^{\infty} (a_m + b_m) I_{l-m}(\lambda\rho_0) e^{-i(l-m)\theta_0} \,. \end{aligned} \tag{67}$$

For $l < 0$ *the translated coefficients are given by*

$$c_l = \sum_{m=l}^{0} a_m \left(\frac{\lambda\rho_0}{2}\right)^{|l-m|} \frac{e^{-i(l-m)\theta_0}}{|l-m|!} \tag{68}$$

and

$$\begin{aligned} d_l = &\sum_{m=-\infty}^{l-1} (a_m + b_m) I_{l-m}(\lambda\rho_0) e^{-i(l-m)\theta_0} \\ &+ \sum_{m=l}^{0} (a_m P_{l-m}(\rho_0) + b_m I_{l-m}(\lambda\rho_0)) e^{-i(l-m)\theta_0} \\ &+ \sum_{m=1}^{\infty} (a_m + b_m) I_{l-m}(\lambda\rho_0) e^{-i(l-m)\theta_0} \,. \end{aligned} \tag{69}$$

A (Q_n, K_n) multipole expansion can be converted into a $(r^{|n|}, P_n)$ local expansion using the following formula:

Lemma 4 *Suppose that*

$$\phi(\mathbf{x}) = \sum_{l=-\infty}^{\infty} \left(a_l Q_l(\rho') + b_l K_l(\lambda\rho')\right) e^{il\theta'} , \tag{70}$$

where (ρ', θ') *are the polar coordinates of* $\mathbf{x}$ *with respect to the point* $\mathbf{x}_0$*, is a multipole expansion of the potential due to a charge density which is contained inside the disk of radius* $R < |\mathbf{x}_0|$ *about* $\mathbf{x}_0$*. Let* (ρ_0, θ_0) *be the polar coordinates of* $\mathbf{x}_0$ *with respect to the origin. Then, for* $\mathbf{x}$ *within the disk of radius* $\rho_0 - R$*, we have*

$$\phi(\mathbf{x}) = \sum_{l=-\infty}^{\infty} \left(c_l P_l(\lambda\rho) + d_l (\lambda\rho)^{|l|}\right) e^{il\theta} , \tag{71}$$

where (ρ, θ) *are the coordinates of* $\mathbf{x}$ *with respect to the origin. For all* l*, we have that*

$$c_l = \sum_{m=-\infty}^{\infty} (-1)^m (a_m + b_m) K_{l-m}(\lambda\rho_0) e^{i(l-m)\theta_0} . \tag{72}$$

For $l > 0$*, we have*

$$\begin{aligned} d_l = &\frac{1}{2^l l!} \sum_{m=-\infty}^{0} (-1)^m (a_m Q_{l-m}(\rho_0) + b_m K_{l-m}(\lambda\rho_0)) e^{-i(l-m)\theta_0} \\ &+ \frac{1}{2^l l!} \sum_{m=1}^{\infty} (-1)^m (a_m + b_m) K_{l-m}(\lambda\rho_0) e^{-i(l-m)\theta_0} . \end{aligned} \tag{73}$$

For $l = 0$*, we have*

$$d_0 = \sum_{m=-\infty}^{\infty} (-1)^m (a_m Q_{-m}(\rho_0) + b_m K_{-m}(\lambda\rho_0)) e^{im\theta_0} \tag{74}$$

For $l < 0$*, we have*

$$\begin{aligned} d_l = &\frac{1}{2^{|l|} |l|!} \sum_{m=-\infty}^{-1} (-1)^m (a_m + b_m) K_{l-m}(\lambda\rho_0) e^{-i(l-m)\theta_0} \\ &+ \frac{1}{2^{|l|} |l|!} \sum_{m=0}^{\infty} (-1)^m (a_m Q_{l-m}(\rho_0) + b_m K_{l-m}(\lambda\rho_0)) e^{-i(l-m)\theta_0} . \end{aligned} \tag{75}$$

Finally, we can shift the center of a local expansion in the $(r^{|n|}, P_n)$. The following translation operator is phrased in terms of a parent and child box, which is the typical setting for an FMM. A child box is any of the four boxes resulting from dividing a parent box into equal square quadrants. We have

Lemma 5 *Suppose that*

$$\Psi(\mathbf{x}) = \sum_{l=-\infty}^{\infty} (a_l P_l(\rho) + b_l (\lambda\rho)^{|l|}) e^{il\theta} , \tag{76}$$

where (ρ, θ) *are the polar coordinates of* $\mathbf{x}$ *with respect to the origin, is a local expansion for a parent box centered at the origin. Let* (ρ_0, θ_0) *be the polar coordinates of the center* $\mathbf{x}_0$ *of a child box with respect to the origin. Then, for* $\mathbf{x}$ *inside the child box, we have*

$$\Psi(\mathbf{x}) = \sum_{l=-\infty}^{\infty} (c_l P_l(\rho') + d_l(\lambda\rho')^{|l|}) e^{il\theta'} , \tag{77}$$

where (ρ', θ') *are the coordinates of* $\mathbf{x}$ *with respect to the child's center* $\mathbf{x}_0$*. For all l, we have*

$$c_l = \sum_{m=-\infty}^{\infty} a_m I_{l-m}(\lambda\rho_0) e^{-i(l-m)\theta_0} . \tag{78}$$

For $l > 0$ *, we have*

$$\begin{aligned} d_l = & \frac{1}{2^l l!} \sum_{m=-\infty}^{l-1} a_m I_{l-m}(\lambda\rho_0) e^{-i(l-m)\theta_0} \\ & + \frac{1}{2^l l!} \sum_{m=l}^{\infty} a_m P_{l-m}(\lambda\rho_0) e^{-i(l-m)\theta_0} \\ & + \sum_{m=l}^{\infty} \binom{m}{l} b_m \rho_0^{|l-m|} e^{-i(l-m)\theta_0} . \end{aligned} \tag{79}$$

For $l = 0$ *, we have*

$$d_0 = \sum_{m=-\infty}^{\infty} a_m P_{-m}(\lambda\rho_0) e^{im\theta_0} + \sum_{m=-\infty}^{\infty} b_m \rho_0^{|m|} e^{im\theta_0} . \tag{80}$$

For $l < 0$ *, we have*

$$\begin{aligned} d_l = & \frac{1}{2^{|l|}|l|!} \sum_{m=-\infty}^{l} a_m P_{l-m}(\lambda\rho_0) e^{-i(l-m)\theta_0} \\ & + \frac{1}{2^{|l|}|l|!} \sum_{m=l+1}^{\infty} a_m I_{l-m}(\lambda\rho_0) e^{-i(l-m)\theta_0} \\ & + \sum_{m=-\infty}^{l} \binom{|m|}{|l|} b_m \rho_0^{|l-m|} e^{-i(l-m)\theta_0} . \end{aligned} \tag{81}$$

With the above translation operators in hand, the new basis functions derived in this paper result in a stable FMM for the modified biharmonic equation. This FMM enables both the fast solution of the system (61) and the fast evaluation of the layer potential (59). Such an FMM has been implemented by the author and the application of that FMM implementation to numerical fluid simulations will be reported at a later date.

6 Conclusion

We have presented new special functions for representing solutions of the modified biharmonic equation on both the inside and outside of a disk. Numerical experiments demonstrate the superiority of using these functions over the naïve approach, which would employ more familiar functions associated with the Laplace and modified Helmholtz equations. Further, we show how such functions can be used to aid in the solution of the modified biharmonic

equation on more complex geometries with an integral equation approach. We also present, in section 5.2, translation operators for multipole and local expansions using our new radial basis functions. These are key components of FMMs [6,16].

The basic approach of the present paper applies to a number of other Green's functions for high-order PDEs, assuming they can be expressed as the difference of Green's functions for lower order PDEs. This includes, for example, the Green's function for the bi-Helmholtz equation (4). Since the essential analysis concerns radial functions only, the approach extends naturally to three dimensions. We will explore these problems in subsequent work.

Acknowledgements T. Askham would like to thank Leslie Greengard for many useful discussions.

Appendix A. Analytical preliminaries

For the Laplace kernel, the original FMM is based on the manipulation of multipole and Taylor expansions. The center of a multipole expansion may be shifted using this formula:

Lemma 6 *(Adapted from Lemma 2.3 of [16].) Suppose that*

$$\phi(z) = a_0 \log(z - z_0) + \sum_{l=1}^{\infty} \frac{a_l}{(z-z_0)^l} \tag{82}$$

is a multipole expansion of the potential due to a charge density which is contained inside the disk of radius R about z_0. Then, for z outside the disk of radius $R+|z_0|$ about the origin

$$\phi(z) = b_0 \log(z) + \sum_{l=1}^{\infty} \frac{b_l}{z^l}\,, \tag{83}$$

where $b_0 = a_0$ and

$$b_l = \left(\sum_{m=1}^{l} a_m z_0^{l-m} \binom{l-1}{m-1} \right) - \frac{a_0 z_0^l}{l}\,, \tag{84}$$

using the standard notation for binomial coefficients. We also have the following bound for the truncation error. With $p \geq 1$,

$$\left| \phi(z) - b_0 \log(z) - \sum_{l=1}^{p} \frac{b_l}{z^l} \right| \leq \frac{F/2\pi}{1-(|z_0|+R)/|z|} \left(\frac{|z_0|+R}{|z|} \right)^{p+1}\,, \tag{85}$$

where F is the L_1 norm of the density.

A multipole expansion may be converted into a Taylor expansion using the following formula:

Lemma 7 *(Adapted from Lemma 2.4 of [16].) Suppose that a charge density is contained inside the disk of radius R about z_0 with $|z_0| > (1+c)R$ for some $c > 1$. Let the multipole expansion due to this density be given as in Lemma 6. Then, this multipole expansion converges inside the disk of radius R about the origin and can be represented by a power series there:*

$$\phi(z) = \sum_{l=1}^{\infty} b_l z^l \tag{86}$$

where,

$$b_0 = \sum_{m=1}^{\infty} \frac{a_m}{z_0^m} (-1)^m + a_0 \log(-z0)\,, \tag{87}$$

and

$$b_l = \frac{1}{z_0^l} \left(\sum_{m=1}^{\infty} \frac{a_m}{z_0^m} \binom{l+m-1}{m-1} (-1)^m \right) - \frac{a_0}{z_0^l\, l}\,, \tag{88}$$

for $l \geq 1$. There is a similar error bound for this lemma, see [16] for details. Suppose that the charge density is supported in a box and the evaluation points z are taken in another. In the case that these two boxes are well separated from each other, we have

$$\left| \phi(z) - \sum_{l=0}^{p} b_l z^l \right| \leq CF \left(\frac{1}{2} \right)^p , \tag{89}$$

where F is as in Lemma 6 and C is a constant.

The center of a Taylor expansion can be shifted using the following formula:

Lemma 8 *(Adapted from Lemma 2.5 in [16]) Let z_0, z, and a_l for $l = 0, 1, \ldots, p$ be complex. Then*

$$\sum_{l=0}^{p} a_l (z - z_0)^l = \sum_{m=0}^{p} \left(\sum_{l=m}^{p} a_l \binom{l}{m} (-z_0)^{l-m} \right) z^m . \tag{90}$$

This formula is exact.

The FMM for the modified Helmholtz kernel is based on the manipulation of expansions in the Bessel functions I_n and K_n. The formula for shifting the center of an expansion in the K_n functions is:

Lemma 9 *(Adapted from [9].) Suppose that*

$$\phi(\mathbf{x}) = \sum_{l=-\infty}^{\infty} a_l K_l(\lambda \rho') e^{il\theta'} , \tag{91}$$

where (ρ', θ') are the polar coordinates of $\mathbf{x}$ with respect to the point $\mathbf{x}_0$, is a multipole expansion of the potential due to a charge density which is contained inside the disk of radius R about $\mathbf{x}_0$. Let (ρ_0, θ_0) be the polar coordinates of $\mathbf{x}_0$ with respect to the origin. Then, for $\mathbf{x}$ outside the disk of radius $R + \rho_0$, we have

$$\phi(\mathbf{x}) = \sum_{l=-\infty}^{\infty} b_l K_l(\lambda \rho) e^{il\theta} , \tag{92}$$

where (ρ, θ) are the coordinates of $\mathbf{x}$ with respect to the origin and the translated coefficients are given by

$$b_l = \sum_{m=-\infty}^{\infty} a_m I_{l-m}(\lambda \rho_0) e^{-i(l-m)\theta_0} . \tag{93}$$

An expansion in the K_n functions may be converted into an expansion in the I_n functions using the formula:

Lemma 10 *(Adapted from [9].) Suppose that*

$$\phi(\mathbf{x}) = \sum_{l=-\infty}^{\infty} a_l K_l(\lambda \rho') e^{il\theta'} , \tag{94}$$

where (ρ', θ') are the polar coordinates of $\mathbf{x}$ with respect to the point $\mathbf{x}_0$, is a multipole expansion of the potential due to a charge density which is contained inside the disk of radius $R < |\mathbf{x}_0|$ about $\mathbf{x}_0$. Let (ρ_0, θ_0) be the polar coordinates of $\mathbf{x}_0$ with respect to the origin. Then, for $\mathbf{x}$ within the disk of radius $\rho_0 - R$, we have

$$\phi(\mathbf{x}) = \sum_{l=-\infty}^{\infty} b_l I_l(\lambda \rho) e^{il\theta} , \tag{95}$$

where (ρ, θ) are the coordinates of $\mathbf{x}$ with respect to the origin and the translated coefficients are given by

$$b_l = \sum_{m=-\infty}^{\infty} a_m (-1)^m K_{l-m}(\lambda \rho_0) e^{-i(l-m)\theta_0} . \tag{96}$$

We phrase the following translation operator in terms of a parent and child box. A child box is any of the four boxes resulting from dividing a parent box into equal square quadrants. The center of an expansion in the I_n functions may be shifted using the following formula:

Lemma 11 *(Adapted from [9].) Suppose that*

$$\Psi(\mathbf{x}) = \sum_{l=-\infty}^{\infty} a_l I_l(\lambda\rho) e^{il\theta} \,, \tag{97}$$

where (ρ,θ) are the polar coordinates of $\mathbf{x}$ with respect to the origin, is a local expansion for a parent box centered at the origin. Let (ρ_0,θ_0) be the polar coordinates of the center $\mathbf{x}_0$ of a child box with respect to the origin. Then, for $\mathbf{x}$ inside the child box, we have

$$\Psi(\mathbf{x}) = \sum_{l=-\infty}^{\infty} b_l I_l(\lambda\rho') e^{il\theta'} \,, \tag{98}$$

where (ρ',θ') are the coordinates of $\mathbf{x}$ with respect to the child's center $\mathbf{x}_0$ and the new local expansion coefficients are given by

$$b_l = \sum_{m=-\infty}^{\infty} a_m I_{l-m}(\lambda\rho_0) e^{-i(l-m)\theta_0} \,. \tag{99}$$

References

1. Abramowitz, M., Stegun, I.A., et al.: Handbook of mathematical functions. Applied mathematics series **55**, 62 (1966)
2. Alpert, B.K.: Hybrid Gauss-trapezoidal quadrature rules. SIAM Journal on Scientific Computing **20**(5), 1551–1584 (1999)
3. Askham, T.: askhamwhat/modbh-paper: v0.0.0 initial draft release (2017). DOI 10.5281/zenodo.997157. URL https://doi.org/10.5281/zenodo.997157
4. Biros, G., Ying, L., Zorin, D.: An embedded boundary integral solver for the unsteady incompressible navier-stokes equations. J. Comput. Phys pp. 121–141 (2004)
5. Bremer, J., Rokhlin, V., Sammis, I.: Universal quadratures for boundary integral equations on two-dimensional domains with corners. Journal of Computational Physics **229**(22), 8259–8280 (2010)
6. Carrier, J., Greengard, L., Rokhlin, V.: A fast adaptive multipole algorithm for particle simulations. SIAM journal on scientific and statistical computing **9**(4), 669–686 (1988)
7. Chapko, R., Kress, R., et al.: Rothe's method for the heat equation and boundary integral equations. Journal of Integral Equations and Applications **9**(1), 47–69 (1997)
8. Chapko, R., et al.: On the combination of rothe's method and boundary integral equations for the non-stationary stokes equation. Journal of Integral Equations and Applications **13**(2), 99–116 (2001)
9. Cheng, H., Huang, J., Leiterman, T.J.: An adaptive fast solver for the modified Helmholtz equation in two dimensions. J. Comput. Phys. **211**(2), 616–637 (2006). DOI 10.1016/j.jcp.2005.06.006. URL http://dx.doi.org/10.1016/j.jcp.2005.06.006
10. Cooley, J.W., Tukey, J.W.: An algorithm for the machine calculation of complex fourier series. Mathematics of computation **19**(90), 297–301 (1965)
11. *NIST Digital Library of Mathematical Functions*. http://dlmf.nist.gov/, Release 1.0.16 of 2017-09-18. URL http://dlmf.nist.gov/. F. W. J. Olver, A. B. Olde Daalhuis, D. W. Lozier, B. I. Schneider, R. F. Boisvert, C. W. Clark, B. R. Miller and B. V. Saunders, eds.
12. Fourier, J.: Mémoire sur la propagation de la chaleur dans les corps solides. Nouveau Bulletin des Sciences de la Société Philomathique de Paris **6**, 112–116 (1808)
13. Garbow, B.S., Cline, A., Meyering, J.: EISPACK, subroutines for eigenvalues, eigenvectors, matrix operations (1993)
14. Gimbutas, Z., Greengard, L.: FMMLIB2D, fortran libraries for fast multipole method in two dimensions, 2011
15. Greengard, L., Kropinski, M.C.: An integral equation approach to the incompressible navier–stokes equations in two dimensions. SIAM Journal on Scientific Computing **20**(1), 318–336 (1998)
16. Greengard, L., Rokhlin, V.: A fast algorithm for particle simulations. Journal of computational physics **73**(2), 325–348 (1987)
17. Helsing, J., Ojala, R.: On the evaluation of layer potentials close to their sources. J. Comput. Phys. **227**(5), 2899–2921 (2008). DOI 10.1016/j.jcp.2007.11.024. URL http://dx.doi.org/10.1016/j.jcp.2007.11.024
18. Jiang, S., Kropinski, M.C.A., Quaife, B.D.: Second kind integral equation formulation for the modified biharmonic equation and its applications. Journal of Computational Physics **249**, 113 – 126 (2013). DOI http://dx.doi.org/10.1016/j.jcp.2013.04.034. URL http://www.sciencedirect.com/science/article/pii/S0021999113003185

19. Kapur, S., Rokhlin, V.: High-order corrected trapezoidal quadrature rules for singular functions. SIAM Journal on Numerical Analysis **34**(4), 1331–1356 (1997)
20. Klöckner, A., Barnett, A., Greengard, L., O'Neil, M.: Quadrature by expansion: a new method for the evaluation of layer potentials. J. Comput. Phys. **252**, 332–349 (2013). DOI 10.1016/j.jcp.2013.06.027. URL http://dx.doi.org/10.1016/j.jcp.2013.06.027
21. Olver, F.W.J., Lozier, D.W., Boisvert, R.F., Clark, C.W. (eds.): NIST Handbook of Mathematical Functions. Cambridge University Press, New York, NY (2010). Print companion to [11]
22. Rachh, M., Klöckner, A., O'Neil, M.: Fast algorithms for quadrature by expansion i: Globally valid expansions. Journal of Computational Physics **345**, 706–731 (2017)
23. Saad, Y., Schultz, M.H.: Gmres: A generalized minimal residual algorithm for solving nonsymmetric linear systems. SIAM Journal on scientific and statistical computing **7**(3), 856–869 (1986)
24. Seeley, R.T.: An introduction to Fourier series and integrals. WA Benjamin (1966)
25. Swarztrauber, P.: FFTPACK, a package of fortran subprograms for the fast fourier transform of periodic and other symmetric sequences (1985)
26. Trefethen, L.N., Bau III, D.: Numerical linear algebra, vol. 50. SIAM (1997)